Conformal-Mapping Design Tools for Coaxial Couplers With Complex Cross Section

Valeria Teppati, *Student Member, IEEE*, Michele Goano, *Member, IEEE*, and Andrea Ferrero, *Member, IEEE*

***Abstract*—Numerical conformal mapping is exploited as a simple, accurate, and efficient tool for the analysis and design of coaxial waveguides and couplers of complex cross section. An implementation based on the *Schwarz–Christoffel Toolbox*, a public-domain MATLAB package, is applied to slotted coaxial cables and to symmetrical coaxial couplers, with circular or polygonal inner conductors and external shields. The effect of metallic diaphragms of arbitrary thickness, partially separating the inner conductors, is also easily taken into account. The proposed technique is validated against the results of the finite-element method, showing excellent agreement at a fraction of the computational cost, and is also extended to the case of nonsymmetrical couplers, providing the designer with important additional degrees of freedom.**

***Index Terms*—Coaxial cables, coaxial couplers, conformal mapping.**

I. Introduction

COAXIAL directional couplers are fundamental components in several microwave applications, where narrow-band and high power-handling capabilities are required [1, Sec. 6.4]. Historically, these devices have been studied with analytical approaches, usually based on conformal mapping (CM), in order to derive closed-form approximate expressions for their characteristic parameters as functions of the geometry [2]. More recently, greater flexibility has been obtained with numerical techniques, especially the finite-element method (FEM), whose main drawbacks are the computational cost and sensitivity of the results to the discretization mesh, particularly important when the FEM is exploited as a parametric optimization tool. A promising alternative, offering at the same time the efficiency of CM and generality of numerical methods, is numerical CM (for a few examples of applications to microwave lines, see [3]–[5]). This paper describes the analysis of coaxial couplers with the Schwarz–Christoffel (SC) formula, a particular CM for polygonal regions, as implemented in the fast, stable, and accurate *SC Toolbox*[1] [6], [7], a public-domain MATLAB[2] package. In principle, this technique may be applied to any coaxial waveguide with one or more conductors and with arbitrary cross section of lines and external shield. Here, a detailed discussion is given first of the classical structures shown in Fig. 1. The generality of the proposed approach is then exploited to study a wider class of geometries, where a metallic diaphragm is inserted between the conductors [see Fig. 2(a)–(c)], and the coupled lines do not have the same cross section [see Fig. 2(d)]. These new geometries are significant for three reasons. First, metallic diaphragms allow a much easier control of the coupling factor than classical configurations. Second, nonsymmetrical structures make it possible to deal with coupled lines having different impedance levels. Third, the additional degrees of freedom provided by these geometries permit to overcome mechanical constraints in the practical realization of narrow-band couplers, and are essential in the design of longitudinally nonuniform broad-band coaxial couplers.

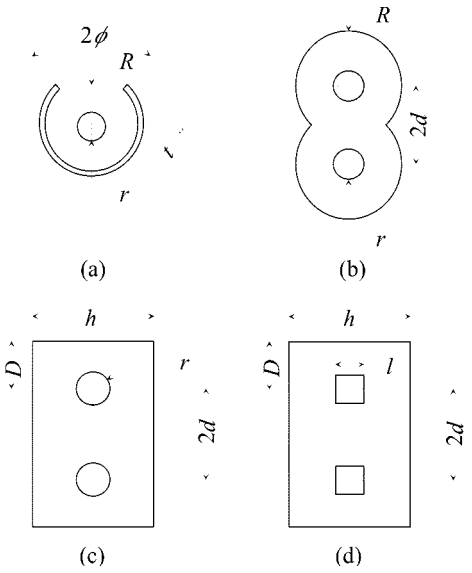

Fig. 1. Coaxial lines and couplers studied with numerical CM analysis. (a) Slotted coaxial line with external shield of arbitrary thickness. (b) Circular coaxial coupler. (c) Rectangular coaxial coupler with circular inner conductors. (d) Rectangular coaxial coupler with square inner conductors.

The paper is organized as follows. Section II describes the application of numerical CM to slotted coaxial lines, an important preparatory step toward the analysis of more complex devices. Section III presents all the necessary steps for the study of symmetrical couplers (i.e., having two orthogonal symmetry planes) with and without diaphragms, together with results for even- and odd-mode characteristic impedances and coupling factors, and comparisons with FEM and available published values. Finally, the most general nonsymmetrical couplers are dealt with in Section IV, and the resulting approach is validated against the symmetrical case and FEM.

Manuscript received July 31, 2001; revised December 12, 2001. This work was supported in part by the Italian National Research Council under the MADESS II Project.

The authors are with the Dipartimento di Elettronica, Politecnico di Torino, I-10129 Turin, Italy (e-mail: valeria.teppati@polito.it).

Digital Object Identifier 10.1109/TMTT.2002.803424.

[1][Online]. Available: http://www.math.udel.edu/~driscoll/SC/.

[2]MATLAB is a registered trademark of The Mathworks Inc., Natick, MA.

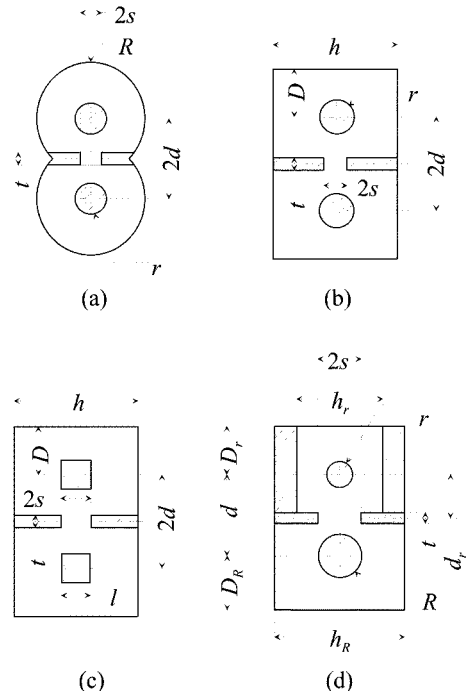

Fig. 2. Coaxial couplers with metallic diaphragms of arbitrary thickness studied with numerical CM analysis. (a) Circular coaxial coupler. (b) Rectangular coaxial coupler with circular inner conductors. (c) Rectangular coaxial coupler with square inner conductors. (d) Nonsymmetrical rectangular coaxial coupler with circular inner conductors.

II. Slotted Coaxial Line

As a first step toward the analysis of coaxial couplers, the application of numerical SC mapping will be described in detail for the slotted coaxial line [see Fig. 1(a)], a simple structure, yet allowing no closed-form expression for its characteristic parameters even under the simplifying assumption of an infinitely thin external shield [8]–[12]. In our approach, following [8], the line is halved by a magnetic wall [see Fig. 3(a)] and the polar symmetry is exploited through a logarithmic transformation $p = \log w$ so that all the segments joining the vertices $w_1, \ldots, w_7$ in the physical domain are mapped into a polygon with two infinite sides. Fig. 3(b) reports the coordinates of all the vertices $\{p_j\}$ and of the corresponding interior angles $\{\pi\alpha_j\}$, which, together, are the only inputs required by SC mapping. The *SC Toolbox* implements both the classical transformation into the upper half-plane z [through the function `hplmap`, see Fig. 3(c)] and the direct mapping into a rectangle, i.e., a parallel-plate capacitor [through the function `rectmap`, see Fig. 3(d)]. In either case, from the results of the numerical transformation, the characteristic impedance of the line may be immediately evaluated as $Z_0 = 1/cC_0$, where C_0 is the per-unit-length capacitance

$$C_0 = 2\epsilon_0 \frac{|\eta_2 - \eta_1|}{|\eta_2 - \eta_3|} = 2\epsilon_0 \frac{K(k)}{K(k')}$$

$$k = \sqrt{\frac{z_2 - z_1}{z_3 - z_1}\,\frac{z_6 - z_3}{z_6 - z_2}}$$

and $K(k)$ is the complete elliptic integral of the first kind [13, Sec. 6.1], $k' = \sqrt{1 - k^2}$, c is the speed of light in vacuum, $\epsilon_0 = 1/\mu_0 c^2$, $\mu_0 = 4\pi \cdot 10^7$ H/m.

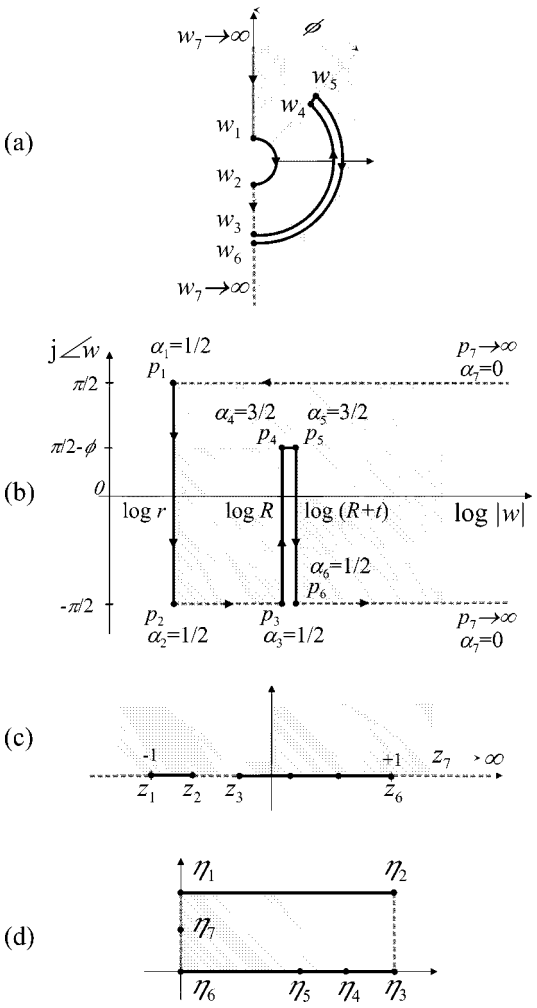

Fig. 3. Mapping of a slotted coaxial line with thick external shield [see Fig. 1(a)]. The polar symmetry of the line is exploited through a logarithmic transformation. The passage from the polygon in the p-plane to the parallel-plate capacitor in the η-plane may be either direct (d) through `rectmap` or (c) through an intermediate transformation into the upper half-plane z with `hplmap`.

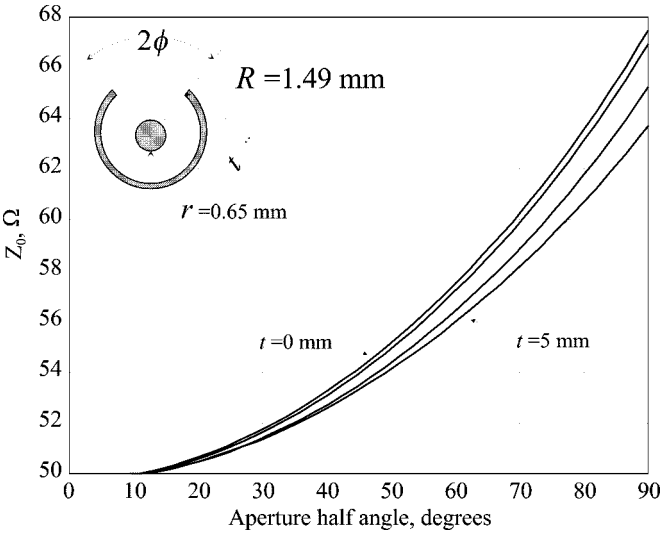

Fig. 4. Characteristic impedance of a slotted coaxial line in air ($r = 0.65$ mm, $R = 1.49$ mm) as a function of the aperture half-angle ϕ for different values of the thickness of the external shield t (0, 0.05, 0.5, and 5 mm).

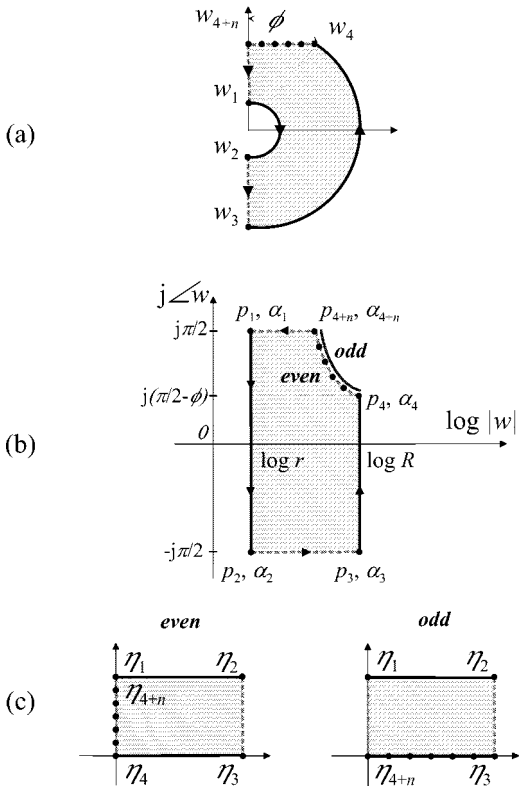

Fig. 5. Mapping of one-quarter of a circular coaxial coupler [see Fig. 1(b)]. The polar symmetry is exploited through a logarithmic transformation. The aperture $w_4, \ldots, w_{4+n}$ is a magnetic wall for the even mode, and an electric wall for the odd mode. Only the direct passage (through `rectmap`) from the polygon in the p plane to the parallel-plate capacitor in the η-plane is shown.

The only difference between thin and thick external shields is that, in the latter case, the polygon in the physical domain has one additional vertex, with no significant impact on the computation time. The effects of the external shield thickness t on the characteristic impedance may be appreciated from Fig. 4, reporting curves of Z_0 as a function of the aperture half-angle ϕ for different values of t.

III. Symmetrical Coaxial Couplers

A. Couplers With Circular Shield

The study of circular symmetrical coaxial couplers [see Fig. 1(b)] requires an inexpensive extension of the technique applied to the slotted coaxial line. Thanks to structural symmetries, only one-quarter of the entire coupler has to be considered [see Fig. 5(a)]. All the sides in the physical domain have finite length, and the only complications arise from the aperture connecting the two circular lines. Since the present version of the *SC Toolbox* cannot deal with curvilinear sides, the aperture is described by introducing $n-1$ extra vertices, so that the corresponding curve $p_4 \cdots p_{4+n}$ resulting from the logarithmic transformation may be well approximated with a many-sided polygon [see Fig. 5(b)]. The vertex coordinates on the aperture may be chosen as

$$p_{4+i} = \log w_{4+i} + \mathrm{j}\left[\frac{\pi}{2} - \phi\,(1 - i/n)\right], \qquad i = 1, \ldots, n$$

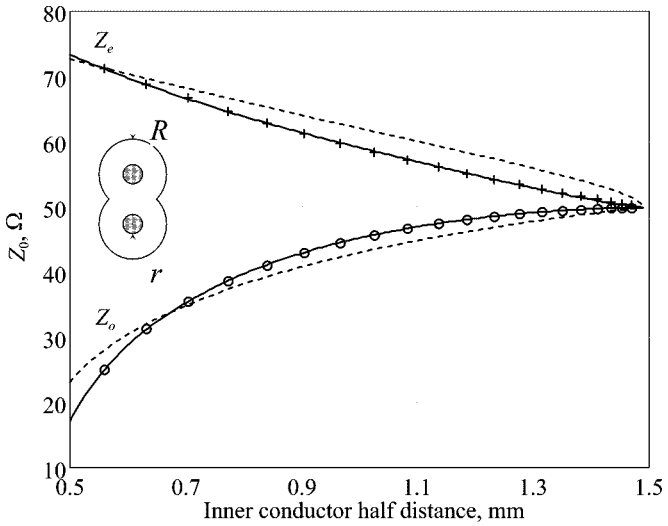

Fig. 6. Even- and odd-mode characteristic impedance of a dielectric-filled circular coaxial coupler as a function of the half-distance d between the inner conductors. The results of numerical CM analysis (crosses, circles) are compared with the values published in [15] (solid lines) and [17] (dashed lines).

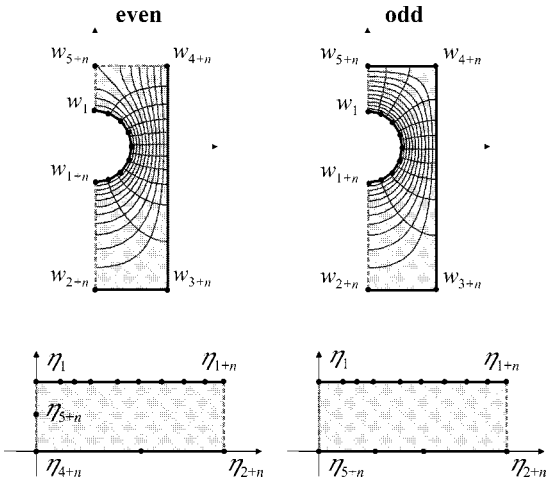

Fig. 7. Mapping of a coaxial coupler with a rectangular shield and circular inner conductor [see Fig. 1(c)]. The polar symmetry is not exploited and the circular conductors are approximated with n-sided polygons. The even-mode (left-hand side) and odd-mode (right-hand side) potential distributions computed with `rectmap` are shown.

where

$$w_{4+i} = \frac{R\cos\phi}{\cos\left[\phi(1 - i/n)\right]}$$

$\phi = \arccos(d/R)$, and the corresponding interior angles are

$$\begin{aligned} \alpha_4 &= \pi - \beta_0 \\ \alpha_{4+i} &= \beta_{i-1} - \beta_i + \pi, \qquad i = 1, \ldots, n-1 \\ \alpha_{4+n} &= \frac{\pi}{2} + \beta_{n-1} \end{aligned}$$

where

$$\beta_i = \arctan \frac{\log w_{4+i+1} - \log w_{4+i}}{\phi/n}, \qquad i = 0, \ldots, n-1.$$

The even- and odd-mode capacitances, C_e and C_o, may be evaluated by considering the aperture as a magnetic or an electric

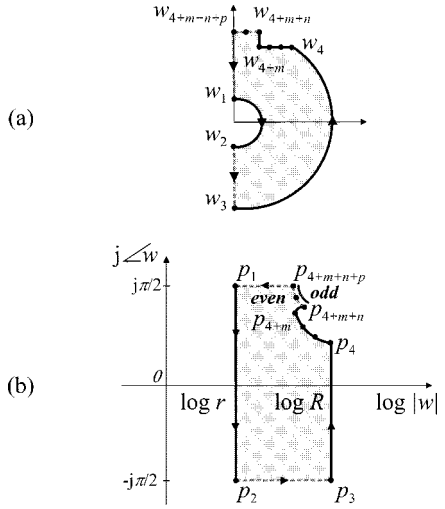

Fig. 8. Mapping of a circular coaxial coupler with diaphragm [see Fig. 2(a)]. The polar symmetry is exploited through a logarithmic transformation. The aperture $w_{4+m+n}, \ldots, w_{4+m+n+p}$ is a magnetic wall for the even mode, and an electric wall for the odd mode.

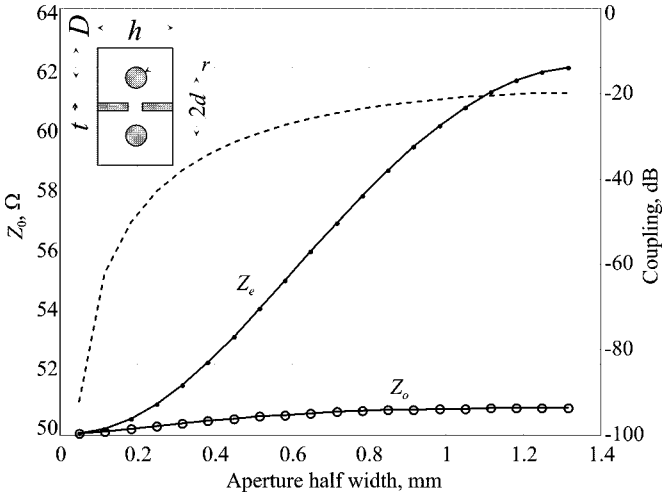

Fig. 9. Characteristic impedances (solid lines, left-hand-side axis) and coupling (dashed line, right-hand-side axis) of a rectangular coaxial coupler in air with diaphragm (circular inner conductors), as functions of the aperture half-width s.

wall, respectively. When `rectmap` is used, the transformations shown in Fig. 5(c) are applied, and C_e, C_o are evaluated from the corresponding sets $\{\eta_i\}_{e/o}$ as

$$C_{e/o} = 2\epsilon_0\epsilon_r \frac{|\eta_2 - \eta_1|}{|\eta_2 - \eta_3|}.$$

From the characteristic impedances $Z_{e/o} = \sqrt{\epsilon_r}/(cC_{e/o})$, the coupling factor may be computed as $\mathcal{K} = (Z_e - Z_o)/(Z_e + Z_o)$ [2], obviously increasing with the aperture angle.

Comparisons with published results for a dielectric-filled coupler ($\epsilon_r = 2.03$, $r = 0.455$ mm, $R = 1.49$ mm, see Fig. 6) demonstrate excellent agreement with interpolation formulas based on FEM computations [14]–[16], as the maximum difference is lower than 0.05%. On the other hand, a previous attempt at closed-form CM analysis [17] leads to discrepancies with both the present approach and FEM-based formulas,

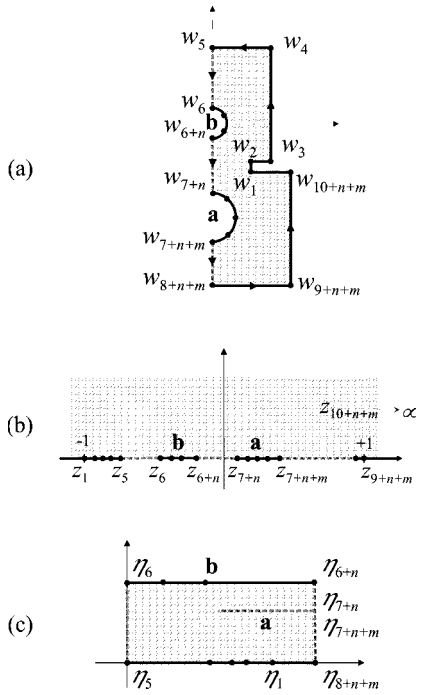

Fig. 10. Mapping of a nonsymmetrical rectangular coaxial coupler with diaphragm [see Fig. 2(d)]. The polar symmetry is not exploited and the circular conductors are approximated with many-sided polygons. The transformation into a two-line ACPW with semi-infinite lateral ground planes via (b) `hplmap` is common for the evaluation of C_a, C_b, and C_{ab}. The final three-conductor mapping for the computation of C_b is shown in (c).

probably because it is not possible to obtain a solution in terms of complete and Jacobi elliptic functions.

For the structure of Fig. 6, the asymptotic dependence of the relative error $\mathcal{E}_{\rm rel}$ on the number of vertices may be modeled as $\mathcal{E}_{\rm rel} \propto \mathrm{e}^{-n/\nu_0}$, with $\nu_0 \approx 5.7$ both for Z_0 and $\mathcal{K}$. Thanks to this exponential convergence rate, the choice $n = 5$ already corresponds to a relative error as small as 0.07% on the characteristic impedances and 0.67% on the coupling.

B. Couplers With Rectangular Shield

In the case of coaxial couplers with rectangular external shields [18] [see Fig. 1(c)–(d)], our CM approach drops the logarithmic transformation and describes the inner conductors as n-sided polygons so that the SC mapping is directly applied to the structure in the physical domain. For the computation of the capacitances and impedances, either `hplmap` or `rectmap` may be exploited, with the same boundary conditions on the aperture used for the circular coupler. As shown in Fig. 7, `rectmap` now allows the direct computation of contour plots of the potential distribution for the even and odd modes. This analysis enables the exact treatment of rectangular structures with polygonal inner conductors. It may also be observed that coupled slab lines [2], [3], [19], [20] are a special type of coaxial couplers with rectangular shields, and their study with the present approach is straightforward.

A convergence study on a coupler with circular inner conductors in air ($r = 0.65$ mm, $h = 2.34$ mm, $D = 4$ mm, $2d = 3$ mm) again demonstrates an exponential convergence rate versus n with $\nu_0 \approx 4.9$. The approximation of the half-

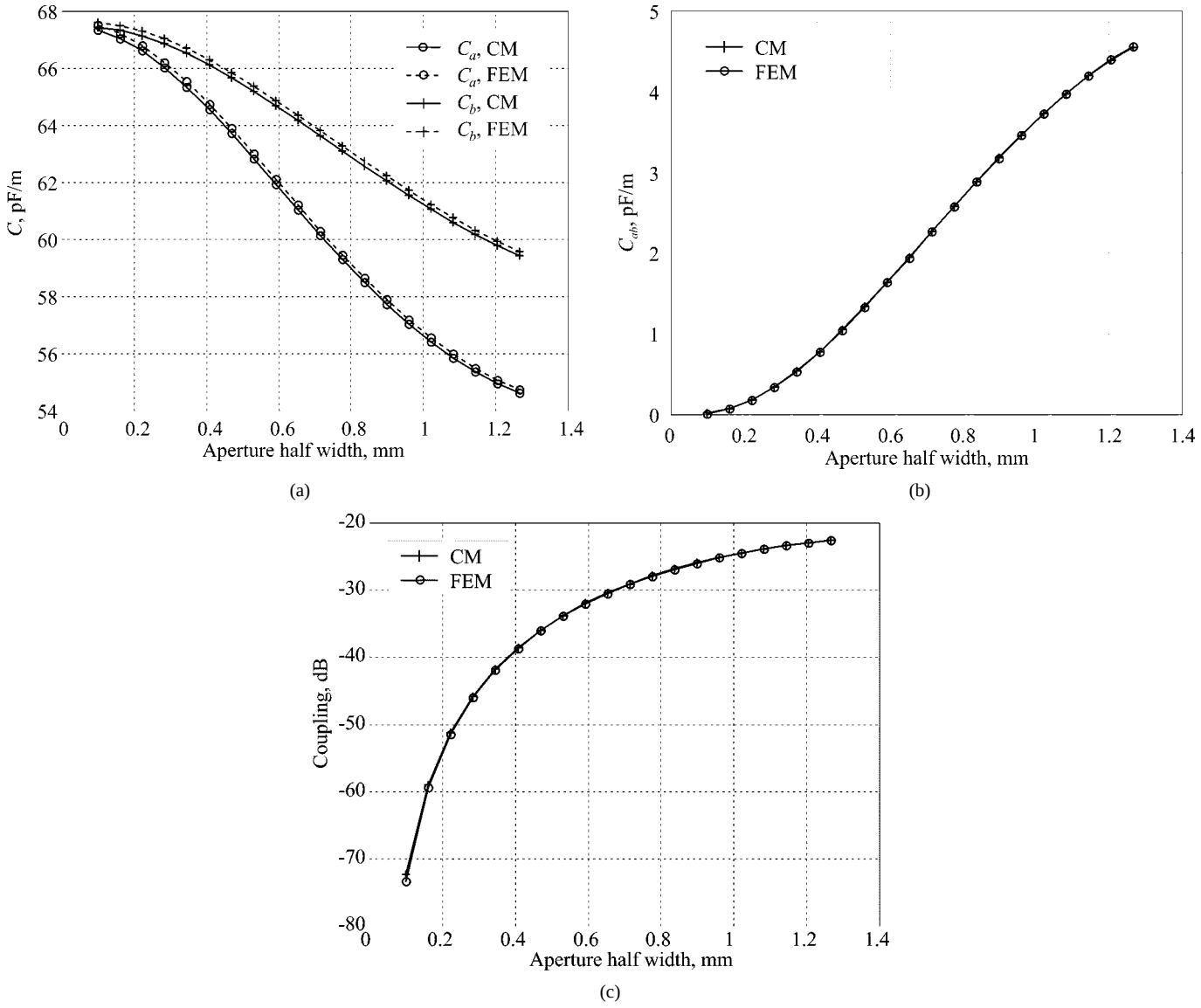

Fig. 11. Comparison of nonsymmetrical multiconductor mapping and FEM on a nonsymmetrical rectangular coupler in air with circular inner conductors. (a) Per-unit-length capacitances C_a and C_b. (b) Per-unit-length mutual capacitance C_{ab}. (c) Coupling factor $\mathcal{K}$ as functions of the aperture half-width s.

circle with a 12-sided polygon yields a relative error of approximately 0.24% on Z_e, Z_o and approximately 0.16% on $\mathcal{K}$. Despite the exponential dependence of $\mathcal{K}$ on the distance $2d$ between the inner conductors, the maximum variation of the coupling factor is smaller than 20 dB, which suggests the need for different structures, such as those proposed in the following sections.

C. Couplers With Diaphragm

The CM procedure can be further generalized to take into account the presence of a metallic diaphragm of arbitrary thickness, partially separating the inner conductors [see Fig. 2(a)–(c)]. Since the width of the diaphragm mainly affects the even-mode impedance, it may be used as the fundamental design parameter in longitudinally nonuniform coaxial couplers in order to effectively control the mode coupling along the longitudinal direction in a much simpler way than with an impractical variation of the distance between the inner conductors. The insertion of a metallic diaphragm may also be useful in narrow-band couplers, especially in the case of a rectangular external shield, because of the much wider range of $\mathcal{K}$ values that can be obtained.

The modifications required to apply the *SC Toolbox* to symmetrical coaxial couplers with diaphragms are illustrated in Fig. 8 in the case of a circular coupler. As a numerical example, Fig. 9 provides plots of Z_e, Z_o, and $\mathcal{K}$ for the structure described in Fig. 2(b) (with $r = 0.65$ mm, $h = 2.63$ mm, $2d = 2.5$ mm, $D = 4$ mm, and $t = 0.1$ mm), as functions of the aperture half-width s. It may be observed that, with such a thin diaphragm, the dependence of Z_o on s is almost negligible, while the variation of Z_e can be larger than 60% and, of course, $\mathcal{K}$ may become arbitrarily small.

IV. Nonsymmetrical Coaxial Couplers

The coupler sketched in Fig. 2(d) is an example of a more general class of structures with less symmetry, which may still be studied with numerical CM for simply connected regions. In

addition to the advantages offered by the metallic diaphragm, nonsymmetrical cross sections allow the coupling between lines of unequal characteristic impedances. Moreover, the use of nonsymmetrical geometries may be the most effective way to overcome mechanical constraints forced, e.g., by the shape and size of standard connectors and by the minimum feasible distance between the inner conductors.

Due to the lack of symmetry between the conductors, the description in terms of even- and odd-mode capacitances must be replaced by the definition of a capacitance matrix [21]

$$\boldsymbol{C} = \begin{pmatrix} C_a + C_{ab} & -C_{ab} \\ -C_{ab} & C_b + C_{ab} \end{pmatrix}$$

where C_a and C_b are the per-unit-length capacitances associated to the inner conductors and C_{ab} is their per-unit-length mutual capacitance. The coupling coefficient $\mathcal{K}$ may be derived from $\boldsymbol{C}$ following the classical formulation by Cristal [21, eqs. (2)–(7), (16)–(26)]. The *SC Toolbox* is now used to map the half-structure bounded by the only remaining symmetry axis [see Fig. 10(a)] into a four-electrode asymmetric coplanar waveguide (ACPW) with semi-infinite lateral ground planes [see Fig. 10(b)]. The capacitance matrix of the ACPW is then readily computed using the Linnér approach [22] [see Fig. 10(c)] in the efficient implementation proposed by Ghione [23].

The resulting technique proves to be very stable and accurate. As a first validation, the nonsymmetrical analysis code is applied to the symmetrical rectangular coupler already examined in Section III-C (see Fig. 9) and compared with the results of a symmetrical CM and FEM. For characteristic impedances, excellent agreement is found between the two CM-based techniques (the maximum difference is lower than 0.05 Ω, having approximated the inner conductors with 20-sided polygons), while FEM results (computed with an adapted triangular mesh having approximately 4000 nodes) show a constant offset of about 0.2 Ω, which may be further reduced with denser meshes. The corresponding coupling factors computed with the three techniques are virtually indistinguishable. Eventually, a comparison between the proposed approach and FEM for a nonsymmetrical coupler ($r = 0.65$ mm, $R = 1.3$ mm, $h_r = 2.63$ mm, $h_R = 5.26$ mm, $d = 3.7$ mm, $D_r = 4$ mm, $D_R = 8$ mm, $t = 0.1$ mm, $d_r = 1.25$ mm) is given in Fig. 11. Once again, tiny mesh-dependent differences between the diagonal elements of $\boldsymbol{C}$ may be noticed, while the corresponding $\mathcal{K}$ is coincident for all practical purposes.

It is worth observing that, although we have limited our study of nonsymmetrical couplers to two-conductor lines with rectangular external shields, the joint application of the *SC Toolbox* and the multiconductor ACPW analysis technique [22], [23] allows the extraction of the characteristic parameters of coaxial structures with an arbitrary number of inner conductors and arbitrary geometries of shield and conductors, as long as a symmetry axis exists.

V. Conclusions

The accurate evaluation of per-unit-length capacitances, impedances, and coupling factors of several coaxial coupling structures has been demonstrated as a simple application of the numerical conformal transformations implemented in the *SC Toolbox*. CM results are in excellent agreement with the FEM, and require a much lower computational cost than the latter technique. The efficiency and user friendliness of the proposed approach allow its use as a design and optimization tool. The most significant feature of the present analysis is the possibility to describe the effects of metallic diaphragms and to study nonsymmetrical structures since these geometries provide important additional degrees of freedom to the design of longitudinally uniform and (potentially broad-band) nonuniform coaxial couplers.

Acknowledgment

The authors would like to thank T. A. Driscoll, Department of Mathematics, University of Delaware, Newark, for his continuous support on the *SC Toolbox*, F. Bertazzi, Dipartimento di Elettronica, Politecnico di Torino, Turin, Italy, for his assistance on FEM validations, S. Gevorgian, Department of Microelectronics, Chalmers University of Technology, Göteborg, Sweden, for useful discussions about the symmetric circular couplers, and G. Ghione, Dipartimento di Elettronica, Politecnico di Torino, Turin, Italy, for his help on ACPWs and nonsymmetrical structures.

References

[1] R. E. Collin, *Foundations for Microwave Engineering*, 2nd ed. New York: McGraw-Hill, 1992.

[2] L. Young, Ed., *Parallel Coupled Lines and Directional Couplers*. Dedham, MA: Artech House, 1972.

[3] E. Costamagna, A. Fanni, and M. Usai, "Slab line impedances revisited," *IEEE Trans. Microwave Theory Tech.*, vol. 41, pp. 156–159, Jan. 1993.

[4] E. Costamagna, "Numerical inversion of the Schwarz–Christoffel conformal transformation: Strip-line case studies," *Microwave Opt. Technol. Lett.*, vol. 28, no. 3, pp. 179–183, Feb. 2001.

[5] M. Goano, F. Bertazzi, P. Caravelli, G. Ghione, and T. A. Driscoll, "A general conformal-mapping approach to the optimum electrode design of coplanar waveguides with arbitrary cross section," *IEEE Trans. Microwave Theory Tech.*, vol. 49, pp. 1573–1580, Sept. 2001.

[6] T. A. Driscoll, "Algorithm 756: A MATLAB toolbox for Schwarz–Christoffel mapping," *ACM Trans. Math. Software*, vol. 22, no. 2, pp. 168–186, June 1996.

[7] ——, *Schwarz–Christoffel Toolbox User's Guide. Version 2.1*. Boulder, CO: Dept. Appl. Math., Univ. Colorado, 1999.

[8] J. Smolarska, "Characteristic impedance of the slotted coaxial line," *IRE Trans. Microwave Theory Tech.*, vol. MTT-6, pp. 161–166, Apr. 1958.

[9] R. E. Collin, "The characteristic impedance of a slotted coaxial line," *IRE Trans. Microwave Theory Tech.*, vol. MTT-4, pp. 4–8, Jan. 1956.

[10] H. A. Wheeler, "Transmission-line conductors of various cross section," *IEEE Trans. Microwave Theory Tech.*, vol. MTT-28, pp. 73–83, Feb. 1980.

[11] P. P. Delogne and A. A. Laloux, "Theory of the slotted coaxial cable," *IEEE Trans. Microwave Theory Tech.*, vol. MTT-28, pp. 1102–1107, Oct. 1980.

[12] E. E. Hassan, "Field solution and propagation characteristics of monofilar–bifilar modes of axially slotted coaxial cable," *IEEE Trans. Microwave Theory Tech.*, vol. 37, pp. 553–557, Mar. 1989.

[13] I. S. Gradshteyn and I. M. Ryzhik, *Tables of Integrals, Series, and Products*, 5th ed. San Diego, CA: Academic, 1994.

[14] H. An, T. Wang, R. G. Bosisio, and K. Wu, "Accurate closed form expressions for characteristic impedance of coupled line with sliced coaxial cable," *Electron. Lett.*, vol. 31, no. 23, pp. 2019–2020, Nov. 1995.

[15] H. An, R. G. Bosisio, K. Wu, and T. Wang, "A 50 : 1 bandwidth cost-effective coupler with sliced coaxial cable," in *IEEE MTT-S Int. Microwave Symp. Dig.*, vol. 2, San Francisco, CA, June 1996, pp. 789–792.
[16] N. Benahmed and M. Feham, "Finite element analysis of RF couplers with sliced coaxial cable," *Microwave J.*, vol. 43, no. 11, pp. 106–120, Nov. 2000.
[17] S. Gevorgian and E. Kollberg, "Conformal mapping based analysis of coupled coaxial lines," in *Proc. 30th Eur. Microwave Conf.*, vol. 2, Paris, France, Oct. 2000, pp. 251–254.
[18] A. Agarwal, C. J. Reddy, and M. Y. Joshi, "Coupled bars in rectangular coaxial," *Electron. Lett.*, vol. 25, no. 1, pp. 66–67, Jan. 1989.
[19] G. B. Stracca, G. Macchiarella, and M. Politi, "Numerical analysis of various configurations of slab lines," *IEEE Trans. Microwave Theory Tech.*, vol. MTT-34, pp. 359–363, Mar. 1986.
[20] S. Rosłoniec, "An improved algorithm for the computer-aided design of coupled slab lines," *IEEE Trans. Microwave Theory Tech.*, vol. 37, pp. 258–261, Jan. 1989.
[21] E. G. Cristal, "Coupled-transmission-line directional couplers with coupled lines of unequal characteristic impedances," *IEEE Trans. Microwave Theory Tech.*, vol. MTT-14, pp. 337–346, July 1966.
[22] L. J. P. Linnér, "A method for the computation of the characteristic immittance matrix of multiconductor striplines with arbitrary widths," *IEEE Trans. Microwave Theory Tech.*, vol. MTT-22, pp. 930–937, Nov. 1974.
[23] G. Ghione, "An efficient, CAD-oriented model for the characteristic parameters of multiconductor buses in high-speed digital GaAs ICs," *Analog Integrated Circuits Signal Processing*, vol. 5, no. 1, pp. 67–75, Jan. 1994.

Valeria Teppati (S'00) received the Laurea degree in electronics engineering from the Politecnico di Torino, Turin, Italy, in 1999, and is currently working toward the Ph.D. degree at the Politecnico di Torino.

Her research interests include microwave device design, measurement techniques, and calibration.

Michele Goano (M'98) received the Laurea and Ph.D. degrees in electronics engineering from the Politecnico di Torino, Turin, Italy, in 1989 and 1993, respectively.

In 1994 and 1995, he was a Post-Doctoral Fellow with the Département de Génie Physique, École Polytechnique de Montréal, Montréal, QC, Canada. In 1996, he joined the faculty of the Dipartimento di Elettronica, Politecnico di Torino. He was a Visiting Scholar with the School of Electrical and Computer Engineering, Georgia Institute of Technology, Atlanta, and with the Department of Electrical and Computer Engineering, Boston University, Boston, MA. He is currently involved in research on coplanar components, optical modulators, and wide-bandgap semiconductor devices.

Andrea Ferrero (S'85–M'85) received the Laurea degree and Ph.D. degree in electronic engineering from the Politecnico di Torino, Turin, Italy, in 1987 and 1992, respectively.

In 1992, he joined the faculty of the Dipartimento di Elettronica, Politecnico di Torino, where he has been an Associate Professor of electronic measurements since 1998. His research activities are in the area of microwave measurement techniques, calibration, and modeling.